International Journal of Heat and Mass Transfer 189 (2022) 122675

Contents lists available at ScienceDirect

International Journal of Heat and Mass Transfer

journal homepage: www.elsevier.com/locate/hmt

Postponement of dynamic Leidenfrost phenomenon during droplet impact of surfactant solutions

Gudlavalleti VVS Vara Prasad [a], Purbarun Dhar [b,*], Devranjan Samanta [a,*]

[a] Department of Mechanical Engineering, Indian Institute of Technology Ropar, Punjab, 140001, India
[b] Hydrodynamics and Thermal Multiphysics Lab (HTML), Department of Mechanical Engineering, Indian Institute of Technology Kharagpur, West Bengal, 721302, India

ARTICLE INFO

Article history:
Received 6 October 2021
Revised 30 December 2021
Accepted 4 February 2022
Available online 11 February 2022

Keywords:
Droplet
Surfactants
Leidenfrost effect
Heat transfer
Boiling
Phase change

ABSTRACT

In this article, a novel method of increasing the dynamic Leidenfrost temperature T_{DL} is proposed by adding both anionic (SDS) and cationic (CTAB) surfactants to water droplets. We focus on understanding the hydrodynamics and thermal aspects of droplet impact Leidenfrost behavior of surfactant solutions and aim to delay the onset of the Leidenfrost regime. The effects of Weber number (*We*), Ohnesorge number (*Oh*), and surfactant concentration on dynamic Leidenfrost temperature (T_{DL}) were experimentally studied in detail, covering a wide gamut of governing parameters. At a fixed impact velocity, T_{DL} was increased with increase of surfactant concentration. T_{DL} decreased with the increase of impact velocity for all solutions of surfactant droplets at a fixed surfactant concentration. We proposed a scaling relationship for T_{DL} in terms of *We* and *Oh*. At temperatures ($\sim$ 400 °C) considerably higher than T_{DL}, droplets exhibit trampoline-like dynamics or central jet formation, associated with fragmentation, depending upon the impact velocity. Finally, a regime map of the different boiling regimes such as transition boiling, Leidenfrost effect, trampolining, and explosive behavior was presented as a function of impact *We* and substrate temperature (T_S). The findings may hold substantial implications in thermal management systems operating at high temperatures.

1. Introduction

Liquid-vapor phase change is ubiquitous in several natural phenomena and man-made utilities. Under its broad aegis, the Leidenfrost effect is an atypical phenomenon where the liquid may levitate above its own vapor cushion at temperatures significantly higher than its boiling point [1]; often observed in day-to-day life when water droplets come in contact with superheated kitchenware. The corresponding temperature at which the onset of the effect occurs is the Leidenfrost point (or temperature). At this juncture, the heat transfer rate between the fluid and the heated surface drops significantly as the vapor cushion formed beneath the fluid droplet is a poor thermal conductor. The impact of liquid droplets on such superheated surfaces is of prime relevance to many industrial processes such as spray quenching of alloys, fire extinguishment by sprinkler systems [2], additive manufacturing, and coatings [3], and turbine blade cooling [4]. The reduction in heat transfer can be detrimental in several such cases, for example, in the thermal management of nuclear power plants [3] or metallurgical treatments. The droplet Leidenfrost effect also has great potential in drag reduction [5] and nanoscale manufacturing processes [6].

In recent times, there have been significant strides in the field of droplet Leidenfrost dynamics. Quere and Clanet et al. have made seminal contributions in this field [1,7-10]. Biance et al. studied the shape of Leidenfrost droplets and their dependence on the dynamics of the vapor layer beneath it [7]. They also characterized the lifetime of the Leidenfrost droplets. Self-propulsion of Leidenfrost drops [8] or solids (those which directly sublimate overheated substrates [9]) can be controlled with specially designed ratcheted surfaces. Directed motion in Leidenfrost drops can be helpful for efficient heat transfer [8–9] and targetted hot-spot cooling. Dupeux et al. [10] incorporated crenulations on the surface to increase friction and control the mobility of Leidenfrost droplets. Bouillant et al. [11] performed particle image velocimetry (PIV) within the Leidenfrost droplets (at 300 °C) and established that mobility is dependent on the droplet sizes. They showed that if the droplet diameters are lesser than the capillary length scale, only one vortex exists within the drop. On the contrary, larger diameter droplets

* Corresponding authors.
E-mail addresses: purbarun@mech.iitkgp.ac.in (P. Dhar), devranjan.samanta@iitrpr.ac.in (D. Samanta).

https://doi.org/10.1016/j.ijheatmasstransfer.2022.122675
0017-9310/

Nomenclature

Abbreviations

CTAB	cetyl trimethyl-ammonium bromide
CMC	critical micelle concentration
D_o	pre-impact droplet diameter (mm)
D_{max}	maximum spreading diameter
DDM	droplet dispensing mechanism
DST	dynamic surface tension
DI water	De-ionized water
g	acceleration due to gravity (m/s^2)
h_{max}	maximum rebounding height
LFP	Leidenfrost point
LFT	Leidenfrost temperature
R	radius of the droplet
SDS	sodium dodecyl sulfate
T_{DL}	dynamic Leidenfrost temperature (° C)
T_s	hot substrate temperature (° C)
T_a	ambient temperature (° C)
U	impact velocity (m/s)

Greek symbols

β_{max}	maximum spread factor
η	dynamic viscosity (mPa-s)
ρ	Density (kg/m^3)
σ_{drop}	equilibrium surface tension (mN/m)
λ_c	capillary length of the droplet (mm)
ϵ	coefficient of restitution

Non-Dimensional parameters

We	Weber number
Re	Reynolds number
Oh	Ohnesorge number
Bo	Bond number

showed the presence of two internal vortices. Shirota et al. [12] explored the relevant length and time scales vital for the transition from the fully wetted to the fully levitated (i.e., Leidenfrost) state of droplets on an isothermal hot substrate using total internal reflection (TIR) imaging technique.

Tran et al. [13] proposed a new scaling relationship for dimensionless maximum spreading (Υ) of impacting droplets on the heated surfaces in both gentle and spray film boiling regimes with Weber number ($\gamma \sim We^{0.4}$). They showed that the spreading dynamics for heated conditions is higher compared to that for ambient conditions ($\gamma \sim We^{0.25}$). Khavari et al. [14] experimentally investigated the impact dynamics of droplets on sufficiently heated surfaces and, based on the fingering patterns of the post-impact droplet, classified the boiling into four regimes, viz. spreading (negligible heating effect), bubbly boiling (activated nucleate boiling at the solid-liquid interface), fingering boiling, and Leidenfrost regime, respectively. Villegas et al. [15] performed direct numerical simulations of the Leidenfrost state. Using the level set and ghost fluid methods, they studied the temporal evolution of drop shapes and vapor layer thickness. Qiao et al. [16] used lattice Boltzmann techniques to simulate the Leidenfrost dynamics of droplets on overheated liquid pools. They explored the effect of various non-dimensional parameters like vapor Stefan number, Bond number *(Bo)*, Ohnesorge number *(Oh)* and releasing height, and pool depth on the Leidenfrost dynamics.

In addition to the research aimed at understanding of fundamental aspects of the droplet Leidenfrost effect, there have been efforts to modulate the dynamic Leidenfrost temperature (T_{DL}) of fluids via the addition of non-Newtonian additives [17–20]. It has been shown by Dhar et al [21] that when long-chain polymers are dissolved in Newtonian fluids, the resultant elastic fluid droplets exhibit rebound suppression on superhydrophobic surfaces. This rebound suppression behavior has been exploited in the case of Leidenfrost droplets to arrest rebound and thereby delay the reduction of heat transfer calibre of the droplets. Secondary atomization of droplets and increase of T_{DL} was observed by Bertola and his co-workers [17–19] with polymer additives in the droplet fluid. Dhar et al. [20] highlighted the role of Weber number and polymer concentration on the Leidenfrost point (LFP). They showed that the long-lasting filaments attached to the substrate are responsible for the increase of T_{DL}. The elastic effects of polymer chains in suppressing the droplet rebound at heated [20] and ambient conditions [21] were explored by Dhar et al. and was shown to be potential method to delay the Leidenfrost effect in droplets.

Another route to morph the T_{DL} is through the addition of surfactants, which can alter the surface tension and the wetting characteristics of the fluid. Qiao and Chandra [22] performed one of the earliest studies on the effect of typical surfactants (sodium dodecyl sulfate, SDS) on drop impact behavior at high surface temperatures. The addition of surfactants enhanced the nucleation of vapor bubbles, reduced bubble coalescence, and promoted foaming in the liquid. An increase in surfactant concentration led to a decrease in the T_{DL}. The surfactants could not affect the evaporation time of the droplets in the film boiling regime, but spray cooling regime was enhanced by addition of surfactants [23]. In contrary to Qiao and Chandra's observations [22], Chen et al. [24] reported the increase of T_{DL} by addition of high alcohol surfactants (HAS). They established an empirical correlation between T_{DL} and the maximum spreading factor. Zhang et al. [25] reported that T_{DL} was reduced by use of SDS and cetyl tri-methyl-ammonium bromide (CTAB), while use of PEG-1000 (a polymer) increased T_{DL}. They concluded that the occurrence of bubble jet and bubble explosion processes on superheated hydrophilic surfaces enhanced the heat transfer efficiency and delayed LFP. Similarly, Moreau et al. [26] showed that Leidenfrost droplets of aqueous solution of SDS at high temperatures undergo violent explosion. The explosion was attributed to the Plateau-Marangoni-Gibbs effect [27].

In this article, we aim to understand the effect of surfactants on the dynamic Leidenfrost phenomenon, when droplets of aqueous surfactant solutions impact superheated substrates. We focus on understanding the intricacies of the hydrodynamics of the processes, which lead to morphed thermal aspects of the Leidenfrost behavior in surfactant solution droplets. In our study, we explore the role of two common laboratory surfactants, SDS and CTAB. Initially, we investigated the role of surfactant concentration, *We, Oh,* and spreading hydrodynamics on the T_{DL} during Leidenfrost boiling ($T_S \sim T_{DL}$) regime. We have invoked the concept of dynamic surface tension (DST) to explain the spreading dynamics. The spreading behavior was counterintuitive where the non-dimensional maximum spread factor (refer Section 3.2) was decreasing in spite of increasing surfactant concentration. Based on the previous studies [31–33], we have invoked the concept of dynamic surface tension (DST) to explain the anomalous spreading dynamics. The T_{DL} was increasing with increase in both SDS and CTAB concentration, which was contrary to earlier studies by Qiao and Chandra [22] and Zhang et al [25]. We have done a comparative study with these existing studies [22,25] and justified our experimental findings. Based on operating impact velocities, at temperatures higher than the T_{DL} ($T_S \sim 400$ °C in the present study), droplets exhibited trampoline-like behavior and a central-jet formation during explosive boiling ($T_S > T_{DL}$). We explore the dynamics of such bouncing and jetting behavior at superheated states with different impact velocities. The role of substrate temperature, Weber number and surfactant concentration on the formation of a central jet at higher temperatures than T_{DL} was reported for the first time, to the best of our knowledge. Finally, we have presented a phase map of the

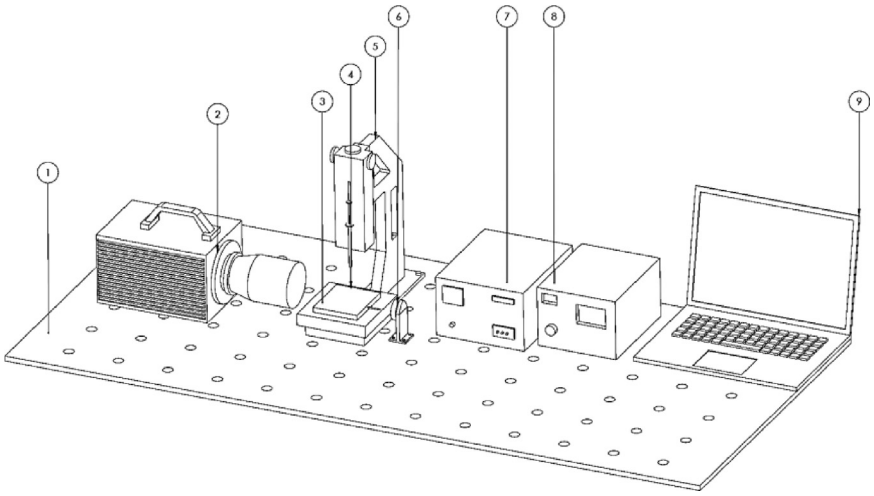

Fig. 1. Schematic of the experimental setup: (1) Vibration free table-top (2) high-speed camera (3) hot substrate (4) microsyringe (5) droplet dispensing mechanism (DDM) unit (6) LED backlight (7) DDM and backlight illumination controller (8) hot substrate controller (9) computer for data acquisition and camera control.

different boiling regimes like transition boiling ($T_S < T_{DL}$), Leidenfrost boiling ($T_S \sim T_{DL}$) and explosive boiling ($T_S > T_{DL}$) as a function of substrate temperature and *We*. We believe that, this study shall provide a comprehensive and mechanistic picture on the delaying of the Leidenfrost effect using surfactant solution droplets.

2. Materials and methods

The experimental setup is similar to our earlier works on droplet impact thermo-hydrodynamics [20,28]. A schematic diagram of the experimental setup is illustrated in Fig. 1. We have used a precision control heater plate (Holmarc Opto-Mechatronics Ltd., India), with digitized temperature control to heat the substrates to temperatures ranging from 150 °C to 400 °C and maintain near isothermal conditions on the substrate during the experiments. The test surface was a square stainless-steel block (80 mm × 180 mm) mounted on the heating element. A T-type thermocouple probe was inserted into the stainless-steel substrate. The thermocouple measured the temperature of the substrate ~1 mm below the top surface and was connected to the digitized temperature controller. The temperature controller can maintain isothermal conditions at the heating element accurate to ±2–3 °C. A height-adjustable droplet dispensing mechanism (Holmarc Opto-Mechatronics Ltd., India) with digitized control was used to release the droplet from different heights, thereby allowing different impact *We* based experiments. A micro-syringe (± 0.1 μl volumetric accuracy) enclosed to the droplet dispenser is used to dispense droplets of fixed volume through a flat head steel needle (22 gage). A high-speed camera (Photron, UK) was used to capture the images of droplet impact on the hot substrate. All experiments were recorded at 4000 frames per second using a 105 mm macro lens (Nikon).

Before each experiment, the stainless-steel hot substrate was properly cleaned with DI water, followed by acetone, to remove dirt and contaminants from the heated surface. The substrate is heated to a particular temperature using the digitized controller and allowed to attain a steady-state. At a steady-state, the substrate temperature may vary within ±2–3 °C of the set value. In this study, DI water, and aqueous solutions of SDS and CTAB (Sigma Aldrich India) were used as fluids. All surfactant solutions were prepared by continuously stirring at 600 rpm with a mechanical stirrer. In this study, we have used different concentrations of surfactant concerning its critical micelle concentration (CMC). We have tested solutions with 0.125, 0.25, 0.5, 0.75 and 1 times the CMC concentration. The relevant thermophysical properties [12,26] of these fluids have been tabulated in Table 1. To characterize the impact hydrodynamics and surface interactions of the impacting droplets, we use certain conventional non-dimensional parameters, as shown in Table 2.

3. Results and discussions

In this section, the drop impact dynamics at high substrate temperatures will be discussed. We have varied the impact *We* by changing the release height of the droplets, the drop sizes, and the surface tension (due to different concentrations of the surfactants). The variation of drop diameters and surface tension was mentioned in Table 2. The impact dynamics behavior has been classified along the lines of previous reports [24,29-30]. The minimum temperature at which the drop levitates over a stable, thin vapor layer without splashing is considered as the Leidenfrost temperature (T_L) [18–24]. When the droplet is gently placed (*We* ~0) over the heated substrate, then the Leidenfrost temperature (LFT) is termed as the static Leidenfrost temperature. However, when a droplet is released from a certain height, the influence of initial impact velocity (quantified through *We*) also becomes an important factor in the Leidenfrost dynamics. Since the LFT changes with the *We,* it is common practice to term it as the dynamic Leidenfrost temperature (T_{DL}) [6,13]. We have considered the T_{DL} as the substrate temperature at which the impacting fluid droplet displays onset of intact rebound off the hot surface, and the corresponding boiling state is denoted as Leidenfrost boiling.

3.1. Influence of substrate temperature on spreading dynamics

The change in surface tension (due to the addition of surfactant) and the thermal condition of the substrate subsequently affect the spreading behavior on the hot surface. As mentioned in earlier studies [3,5-6] on many applications, it is essential to understand the spreading dynamics to estimate the heat transfer rate of droplets during the Leidenfrost stage. This section shall discuss how surfactant concentration and substrate temperature interplay to bring about changes in the spreading hydrodynamics. Fig. 3a and b illustrate the maximum spread state of impacting DI water and surfactant droplets on a substrate at ambient temperature T_{DL} ~30 °C, and at their respective dynamic Leidenfrost temperatures

Table 1
Experimental conditions and thermophysical properties of test fluid droplets: pre-impact droplet diameter D_O (mm), density ρ (kg/m^3), surface tension σ (mN/m), viscosity η (mPa-s), and capillary length λ_c (mm). In Table 1 CMC represents critical micelle concentration.

Liquid	D_o	ρ	σ	η	λ_c
DI water	2.64	995.67	71.03	0.791	2.69
SDS (0.125 CMC –1 CMC)	2.55 – 2	972.15 - 1010	67.725 - 39.8	0.792 - 0.802	2.66 – 2.0
CTAB (0.125CMC – 1 CMC)	2.53–2.34	994 - 994.25	49.31 - 33.53	0.731–0.732	2.24 - 1.85

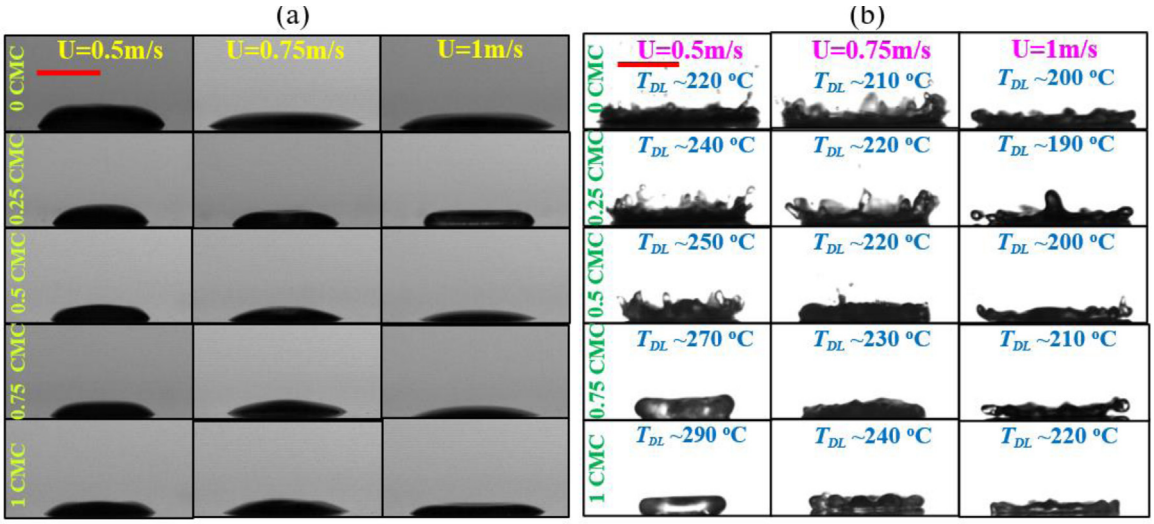

Fig. 2. Maximum spread state of SDS droplets for different impact velocities at (a) T_a ~30° C, and (b) at their respective T_{DL} s (has been shown in the inset of each cell). The scale bar represents ~2.64 mm. The maximum spreading diameter (D_{max}) measurements with varying Weber number and surfactant concentration are shown in Supplementary information (fig. SI- 2). The transient dynamics of SDS droplets at 220° C (the temperature at which a water droplet attains Leidenfrost state at 0.5 m/s in the present study) is provided in fig. SI-1.

Table 2
List of dimensionless parameters used: ρ, U, D_o, σ, D, t, R and Re represent density, impact velocity, pre-impact diameter, surface tension, spreading diameter, spreading time, radius of the impacting surfactant droplets and Reynolds number respectively.

Dimensionless parameter	Expression	Range of values
Weber number	$We = (\rho U^2 D_o)/\sigma_{drop}$	9.2 – 49.78
Ohnesorge number	$Oh = \sqrt{We}/Re$	0.0015 – 0.0030
Bond number	$Bo = (\rho g {D_o}^2)/\sigma_{drop}$	0.82 – 0.96
spread factor	$\beta_{max} = D_{max}/D_o$	1.0 – 2.8

(T_{DL}) respectively. In this context, it must be noted that due to variation in equilibrium surface tension, the droplet diameter varies with the surfactant concentration (droplet size impacting the surface decreases with an increase in surfactant concentration).

As seen from Table 1, the highest concentration (1 CMC SDS) has a droplet diameter ~2 mm, whereas the lowest concentration (0.125 CMC SDS) solution has a droplet diameter of ~2.5 mm. At 0 CMC (i.e., water) the droplet diameter is ~ 2.6–2.7 mm. Since the initial drop diameters are different, it is cumbersome to quantify the effect of surfactants on the spreading diameter directly from Fig. 2. However, the effect of impact velocity for a fixed surfactant concentration is readily evident from Fig. 2. For a fixed surfactant concentration, maximum spreading diameter increases with increased impact velocity at both ambient conditions and at the corresponding Leidenfrost state. It is noted from Fig. 2b that compared to water at its Leidenfrost state, the tendency of crown formation and fragmentation of secondary droplets decreases with the addition of surfactants. We further note that the vigorous boiling during impact at the corresponding Leidenfrost state is reduced with surfactants, as evident from the reduction in the splashing behavior at impact (Fig. 2b, 1st column).

3.2. *Influence of* We *and surfactant concentration on spreading dynamics during Leidenfrost boiling* (T_{DL})

As both maximum spreading diameter (D_{max})and initial droplet diameter (D_o)changes with increasing surfactant concentration, we have quantified the spreading dynamics by defining the non-dimensional maximum spread factor ($\beta_{max} = D_{max}/D_o$). This section highlights the role of *We* on the spreading dynamics at the Leidenfrost state of each fluid i.e., at T_{DL}. The *We* based on impact velocity at the moment of impact is governed by the droplet release height, droplet diameter, as well as surface tension. For the sake of simplicity, we have considered the equilibrium surface tension at ambient temperature [24] for calculation of the *We*. Fig. 3(a) and (b) show the variation of β_{max} for different concentrations (0 to 1 CMC) of both SDS and CTAB solution droplets at their respective T_{DL} over different *We*. For a given test fluid, the *We* is increased by increasing the drop release height. Consequently, the β_{max} (for a particular fluid) also increases due to the dominance of the stored kinetic energy of impacting fluid droplet against the surface energy.

From Fig. 3a and b, it is observed that β_{max} decreases with an increase of surfactant concentration, at a particular *We*. The decreasing trend of spreading diameter with increasing surfactant concentration (which reduces equilibrium surface tension) is counterintuitive [20,29-30]. Recent studies have shown the role of dynamic surface tension (DST) in the case of determining maximum spreading [31–32]. These studies have put forward that during the fast-spreading dynamics (occurring in the order of milliseconds), the DST should be considered instead of the equilibrium surface tension. In the initial phase after impact on the substrate, the surfactant molecules require certain time to diffuse from the bulk of the drop to the recently formed interfaces to initi-

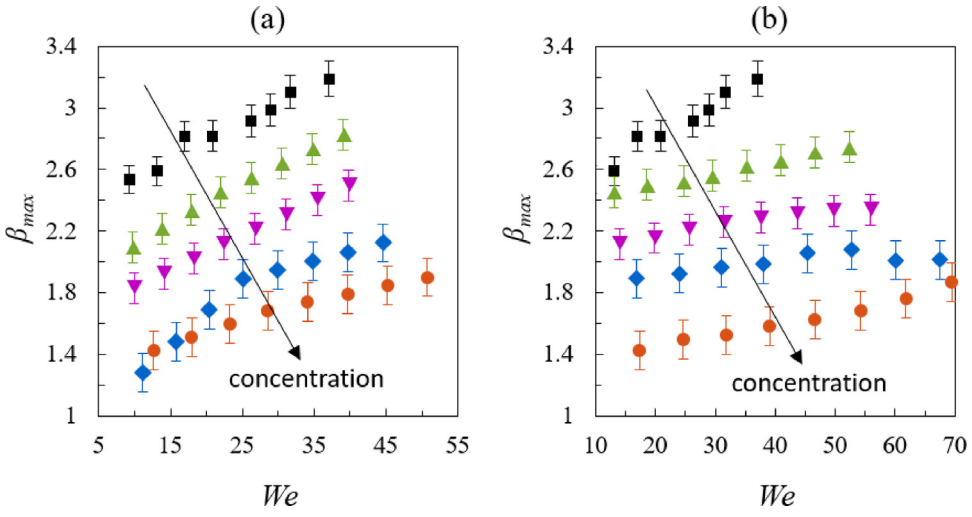

Fig. 3. The maximum spread factor ($\beta_{max} = D_{max}/D_o$) at different *We* for surfactant solution droplets of (a) SDS (b) CTAB, respectively. In above figures, (■) represents 0 CMC or water, (▲), (▼), (♦) and (●) represent surfactant concentrations of 0.25 CMC, 0.5 CMC, 0.75 CMC and 1 CMC, respectively. The arrows represent increasing surfactant concentration. Fig. SI-3 (supplementary information) shows the variation of β_{max} for different impact velocities.

ate the process of reduction in surface tension. The surface tension in this phase could be higher than the equilibrium surface tension with surfactants. We can interpret the equilibrium surface tension as the steady state value surface tension value for non-deforming interfaces whereas DST is the instantaneous surface tension for the temporally varying interfaces. The temporal evolution of the freshly formed interfaces is referred as surface aging. Since the timescale for attainment of equilibrium surface tension values is higher than the time scale of spreading dynamics, the role of DST in spreading dynamics is important. The surfactants were categorized as "*fast*" and "*slow*" depending upon the adsorption-desorption kinetics of the surfactant molecules from the bulk of the fluid to the liquid-air interface and resultant transient reduction in surface tension. The role of DST on maximum spreading is more prominent at higher impact velocities [33]. At higher impact velocities it was observed that maximum spreading diameter of the surfactant solution droplets were less than that of water drops. Previous studies [33] have suggested that for high impact velocities and resultant smaller time scale of spreading process, the occurrence of non-uniform distribution of surfactant molecules at the air-liquid interface may give rise to Marangoni stresses, which may impede the process of droplet spreading.

CTAB was shown to be a "*slow*" surfactant in a study by Hoffman et al. [31]. Based on these studies, we hypothesize that both the surfactants (CTAB and SDS) used in our experiments are "*slow*" to reduce the interfacial force, thereby failing to increase D_{max} to the intuitive levels at their respective dynamic Leidenfrost temperatures (T_{DL}). In addition to the potential role of DST [31–33], the atypical decreasing trend of spreading factor with increasing surfactant concentration may also be due to thermo-capillarity driven Marangoni flows [34–37]. Due to the high-temperature gradient between the bottom and top surface of the droplets at the $T_{DL,}$ and the resultant surface tension gradient, a toroidal convection sets in the droplet [36]. Fluid motion starts along the spherical periphery and sequentially accelerates downward to the contact point near the center. This internal convection impedes the spreading process, as the flow tries to curl up in the opposite direction instead of advancing horizontally towards the spreading contact line. Hence, we believe that such thermo-capillarity induced internal and interfacial convection becomes stronger with increasing surfactant concentration (due to additional solutal Marangoni effect [38,39]) and results in the decreasing trend of spreading factor with increasing surfactant concentration for a fixed *We*.

3.3. Role of surfactant concentration on dynamic Leidenfrost temperature (T_{DL})

The dependence of dynamic Leidenfrost temperature (T_{DL}) on surfactant concentration is discussed in this section. Fig. 4(a) and (b) illustrate the side view and top view of the impact dynamics of various concentrations of SDS droplets at their corresponding Leidenfrost state. From Fig. 4, it can be readily observed that at a fixed velocity of $U = 0.5$ m/s, the time to attain the maximum spreading diameter decreases with the increase of surfactant concentration. This effect is obvious as the droplet size decreases with the increase in surfactant concentration (refer Table 1). The residence time (time from moment of impact to onset of lift-off) decreases with the surfactant concentration (4th column of Fig. 4a, b). The Leidenfrost temperature T_{DL} was denoted as the temperature at which the droplet showed rebounding off the surface for the first time [20]. At a slightly lower temperature than T_{DL}, the droplets were in always contact wholly or partially with the heated substrate. The droplets, with increasing surfactant concentration, exhibit mode shapes characterized by an undulating interface (Fig. 4b, 2nd and 3rd column). Such prominently distorted interface during the spreading and boiling phenomena is akin to the Taylor-Marangoni instability discussed in the literature [40]. In the present case, the presence of the surfactants augments the thermal Marangoni instability due to the addition of the solutal counterpart, which leads to such prominently distorted interface of the droplet due to thermo- and soluto-capillary disturbances.

Fig. 5a, and b show the variation of T_{DL} with variation of impact velocity and surfactant concentration, for both SDS and CTAB solution droplets, respectively.

For a fixed impact velocity, T_{DL} increases with an increase in surfactant concentration. The increasing trend is more prominent for SDS solutions (Fig. 5a). At the lowest impact velocity (0.5 m/s), the T_{DL} for 1 CMC SDS solution is higher than water droplets by almost ~70 °C, which is a high delay of the onset of Leidenfrost effect, and may have strong implications for several utilities. In the case of CTAB solutions, T_{DL} initially increases with increasing surfactant concentration up to 0.25 CMC and then maintains a near-constant value at a higher temperature compared to water (0 CMC) (Fig. 5b). For both the solutions, at fixed surfactant concentration, T_{DL} decreases with an increase in impact velocity. This trend is similar to the Leidenfrost phenomena studies with water and polymer droplets [20]. With an increase in impact velocity,

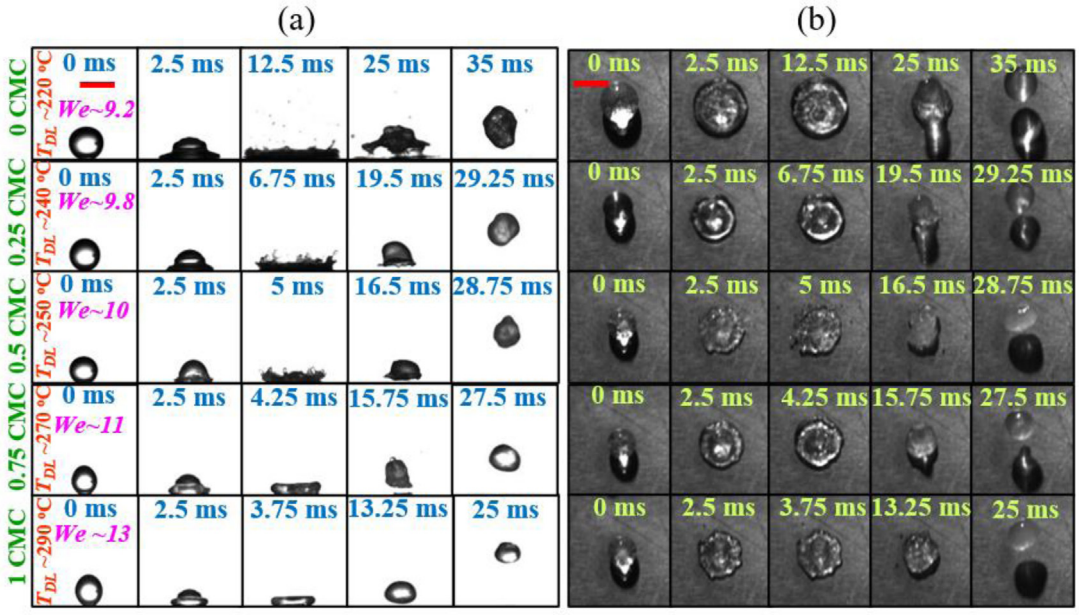

Fig. 4. Temporal evolution of the impacting SDS solution droplets with low impact velocity $U = 0.5$ m/s at their respective T_{DL}: (a) side view (b) top view. For the same initial impact velocity, *We* is changing mildly due to variation in surfactant concentration. The scale bar represents 2.64 mm. The 3rd column of each row represents the instant at which maximum spread occurs. The 4th column of each row represents the instant at which the droplet begins to levitate for the first time.

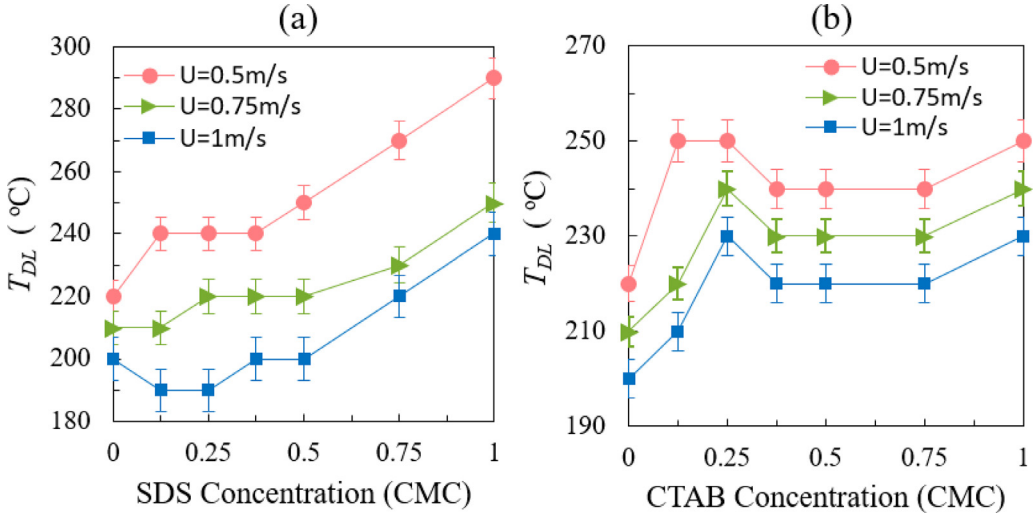

Fig. 5. The dynamic Leidenfrost temperature (T_{DL}) over surfactant concentration of (a) SDS and (b) CTAB fluid droplets.

due to higher inertia, droplets spread to a greater distance radially (as long as the impact velocity is low enough not to induce splashing/fragmentation). The subsequent increase in the contact area between the spreading droplet and the heated surface promotes the formation of nucleation sites at the liquid-solid interface to form vapor pockets. The enhanced rate of vapor formation beneath the drop helps in stable vapor layer formation and results in droplet levitation above it. Hence with increasing impact velocity, the propensity for attaining Leidenfrost state onsets at a lower temperature [20]. Following this argument, the increasing trend of T_{DL} with an increase in surfactant concentration can be explained. Since on heated surfaces, the radial spreading is observed to decrease with the surfactant concentration, the propensity of achieving the Leidenfrost state also reduces compared to water.

Our findings are in contrast with previous studies where T_{DL} was observed to decrease with increasing concentrations of SDS [22,25] and CTAB [25]. One of the possible reasons could be the type of substrate. We have performed the Leidenfrost dynamics experiments on smooth stainless steel whereas previous studies were done on unmodified and modified (trimethoxy silane) smooth silicon surfaces [25]. However, this reasoning is inconclusive as the types of surfaces (smooth stainless steel) were similar for our studies and work by Qiao and Chandra [22]. Another reason could be the variation in droplet size. The previous studies had droplets of diameter ~2.05±0.03 mm [22] and 2 mm [25] whereas our experiments involved greater variation (0.125CMC and 1CMC SDS droplets were of 2.55 mm and 2 mm diameter respectively. We have tried to perform the experiments with the droplet sizes selected in such a way that the capillary and gravitational effects are almost balancing one another. For droplets size less than capillary length (λ_c), the droplets can retract easily and assume the spherical shape [41] quickly. Due to lower contact surface area as well as contact time with the heating substrate, the vapor can easily cushion the droplet and attains dynamic Leidenfrost stage at a lower temperature. Similarly, if the droplet size is more than its λ_c, due to greater effect of gravitational force over capillary force, droplets tend to form puddle structure in the spreading state and has lesser propensity to assume a spherical shape during retraction [7]. Due

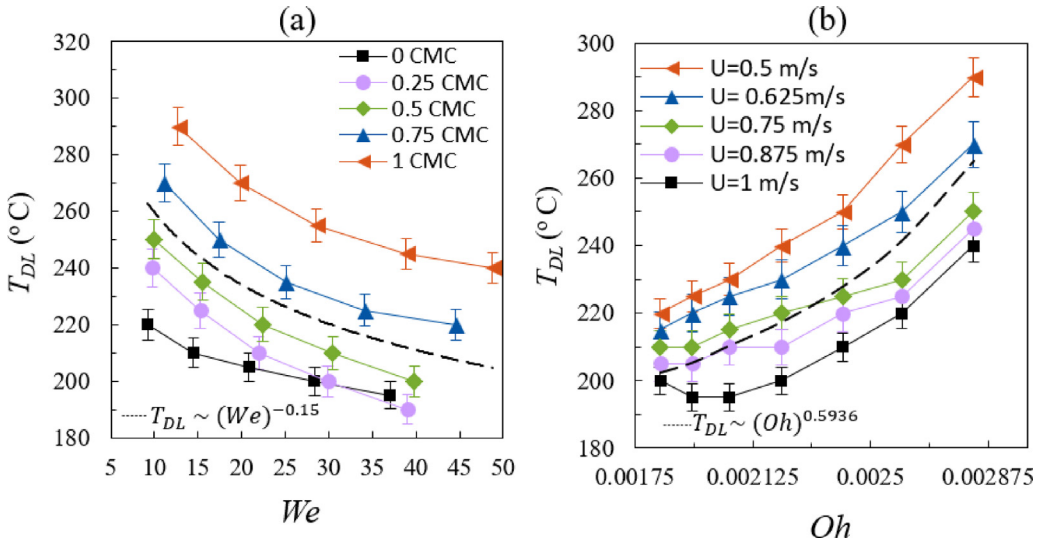

Fig. 6. Dynamic Leidenfrost temperature (T_{DL}) with respect to (a) Weber number *(We)* and (b) Ohnesorge number *(Oh)* for SDS solution droplets. The black dotted lines (**––**) in(a) and (b) represents the scaling behavior of T_{DL} with *We* and *Oh* respectively (as per given scaling in each figure).

to higher area of the flattened puddle structure, it is difficult for vapor to levitate the droplet. Consequently the dynamic Leidenfrost state is achieved at a higher temperature. For instance, the capillary length (λ_c) of SDS droplet with 0.125 CMC is 2.66 mm (refer Table 1). If we operate the same 0.125 CMC SDS droplet with diameter of 2 mm, the droplet will attain spherical shape easily during retraction and achieve the Leidenfrost state at lower temperature due to the predominance of capillary effects. Moreover, if we maintain all SDS surfactant droplets with diameter of 2 mm [22,25] for all concentrations, for most of the concentrations it will be gravity dominated regime. Hence, we operated all concentrations of both SDS and CTAB surfactant droplets near capillary length scale (i.e., 0.125CMC SDS droplet operating diameter D = 2.55 mm, which is very near to its capillary length scale, i.e., 2.66 mm).

For further insight, we emphasized the influence of Bond number (mutual competition between both capillary forces and gravitational forces) on T_{DL} in the section3.5. The droplet sizes were reducing with the increase in surfactant concentration. The variation of Bond number due to size variation may be another potential reason for the contrasting results. In addition, although the equilibrium surface tension for a specific type of surfactants are generally same, the role of DST in the first few milliseconds may vary from one batch of surfactants to another as the manufacturers were different in each other (Sigma Aldrich for our studies, Malinckrodt Speciality Chemicals [22] and Shanghai Aladdin Biochemical Technology Co., Ltd [25]).

3.4. Scaling T_{DL} with Weber (We) and Ohnesorge (Oh) numbers

Subsequently, based on the information highlighted in Fig. 5a and b, the dependence of T_{DL} on *We* for SDS solution droplets is shown in Fig. 6(a). It is evident that the T_{DL} decreases with an increase of *We* for all solution concentrations. Since the β_{max} (refer Fig. 4) increases with the increase of *We*, heat transfer from the hot substrate occurs over a larger area of the thin liquid disk formed by the droplet at maximum spread state. As a result, the formation of a stable vapor cushion is more favorable at lower temperatures, resulting in decreasing trend of T_{DL} with increasing *We*. At the same *We*, the T_{DL} increases with an increase of surfactant concentration. This reveals that *We* alone is not enough to explain the effect of surfactant concentration on the T_{DL}. To improve upon this observation, we introduce another non-dimensional number, the

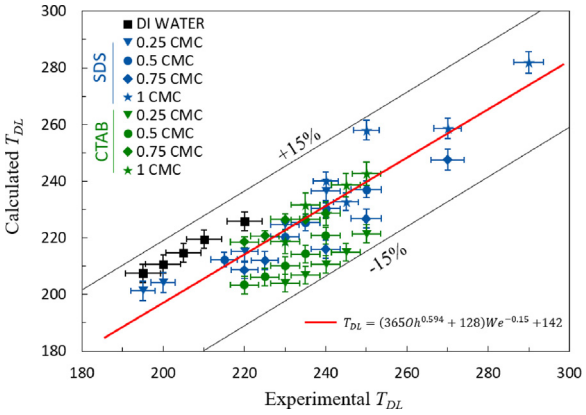

Fig. 7. Comparison between the calculated and experimental T_{DL} of impacting surfactant solution droplets with different concentrations.

Ohnesorge number ($Oh = \frac{\mu}{\sqrt{(\rho\sigma D)}} = \frac{\sqrt{We}}{Re}$). *Oh* is the ratio of viscous forces to both surface tension and inertial forces. Fig. 6 (b) reveals that T_{DL} vs. *Oh* reflects the increasing trend of T_{DL} with surfactant concentration at a fixed impact velocity (Fig. 7) as in both cases, the equilibrium surface tension decreases with the increment of *Oh* and surfactant concentration. From Fig. 6, it is visually evident that T_{DL} is dependent on both *We* and *Oh*. Analogous to a previous study of the Leidenfrost effect with high-alcohol surfactants (HAS) [24], we have attempted to introduce a scaling relationship of T_{DL} with *We* and *Oh*.

The T_{DL} converges to static Leidenfrost temperature (T_{SL}), when *We* approaches zero. The experimental results of T_{DL} are fit to conform to the following relationship: $T_{DL} = (aOh^b + c)We^{-d} + e$. Through least squares regression, the scaling correlation of T_{DL} in terms of *We* and *Oh* (with ±15 % confidence interval, refer Fig. 7) is obtained as: $T_{DL} = (365Oh^{0.594} + 128)We^{-0.15} + 142$. We believe that this scaling correlation will be of valuable reference for future researchers in this field.

3.5. Influence of Bond number (Bo) on T_{DL}

From the expression of Bond number, $Bo = \frac{\rho g D_o^2}{\sigma}$, it is evident that there are two parameters (D_o and σ) which are varying

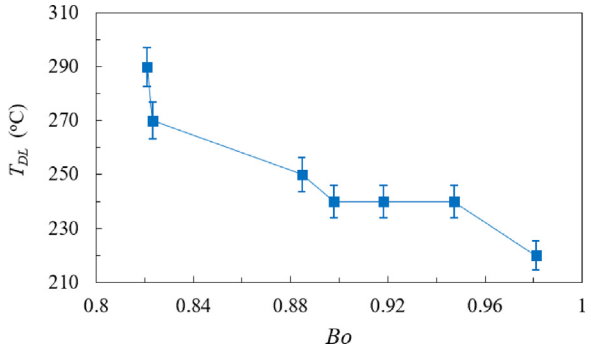

Fig. 8. Effect of Bond number (*Bo*) on dynamic Leidenfrost temperature T_{DL} of different concentrations of SDS solution droplet at impact velocity $U = 0.5$ m/s.

with surfactant concentrations. With increasing surfactant concentration, the equilibrium surface tension value decreases. Since σ is in the denominator, due to its decreasing nature with increasing surfactant concentration, *Bo* values will increase if other parameters are same. On the other hand, due to reduction in equilibrium surface tension, our initial diameters of the droplets hanging from the syringe were also decreasing. As D_o is in the numerator, *Bo* will decrease with increase in surfactant concentration, provided other parameters are constant. Due to this contrasting impact of these two quantities on Bond number, the dependence of *Bo* during the levitation state at T_{DL} on varying concentrations at a fixed impact velocity $U = 0.5$ m/s is presented in Fig. 8. In Fig. 5, it was already observed that the T_{DL} increases with the surfactant concentration. Due to reduced droplet diameters for higher surfactant concentration, *Bo* is decreasing with increasing surfactant concentration, in spite of the reduction in equilibrium surface tension. As a result, Fig. 8 highlights that T_{DL} decreases with increasing *Bo*. This figure may provide relevant information on the dynamics of the Leidenfrost droplets only in terms of the droplet and its physical properties.

3.6. Trampolining dynamics of the droplet at (T_s>T_{DL}) ~400° C

At temperatures significantly higher than T_{DL} (i.e., at $T_S \sim 400$ °C in the present discussion), droplet impact behavior is significantly changed with impact velocity. Similar to the rebound height at T_{DL} s (SI-4), rebound height reduces with increasing impact velocity for 0.5 m/s. At lower impact velocity ~0.5 m/s, droplets display a series of bouncing off dynamics on the substrate. This type of behavior is termed trampolining dynamics, as described in the literature [9,11,20,40]. On the further increase of impact velocity to 1 m/s, a central jet formation and ejection was observed during the retraction phase. In this section, we will discuss trampolining behavior. The time-dependent bouncing behavior of the droplets at different SDS concentrations is presented in Fig. 9. At significantly high temperature ~400 °C, prompt formation of the stable vapor layer (just after ~10 ms, refer to 3rd and 4th column of Fig. 9) enhances the cushioning effect, and the rapid vapor generation leads to the ejection of the droplet from the surface in a nearly intact manner. The sustained oscillations are possible due to the thermocapillarity induced flow and vapor generation during the contact, energizing the flow [36–40]. This is a significant deviation from the impact dynamics at their corresponding T_{DL} (refer to fig. SI-4). At T_{DL}, for all impact velocities, droplets rebounded off the surface. For a fixed test fluid, rebound height decreased with increasing impact velocity. This is consistent with a previous study, highlighted [42] the increase of viscous dissipation and the resultant reduction in retraction kinetic energy with increasing impact velocity.

Subsequently, the non-dimensional rebound height (rebound height/drop radius) for the 1st rebound and the coefficient of restitution (rebound height/initial height)$^{0.5}$ for 0.5, 0.625, and 0.75 m/s were presented in Fig. 10a and b, respectively. We have tried to observe the trampolining behavior at impact velocity lesser than 0.5 m/sec. However, for lower velocity like 0.4 m/sec, the needle is too close to the substrate. For example, at 0.4 m/sec, the equivalent distance from the needle tip is around 8.15 mm. The water droplets are of 2.64 mm diameter. The remaining 5.51 mm height was insufficient to avoid the disruption of trampolining behavior by the needle. As a result, we haven't reported the measurements for lower impact velocities. At velocities higher than 0.75 m/s and $T_s \sim 400$ °C, for some surfactant concentrations, instead of trampolining dynamics, the drops displayed jet formation and fragmentation. So, we have reported for a limited range of impact velocities of 0.5 to 0.75 m/sec. The non-dimensional rebound height for 0.5 and 0.625 m/sec initially decreases at 0.25 CMC and then in-

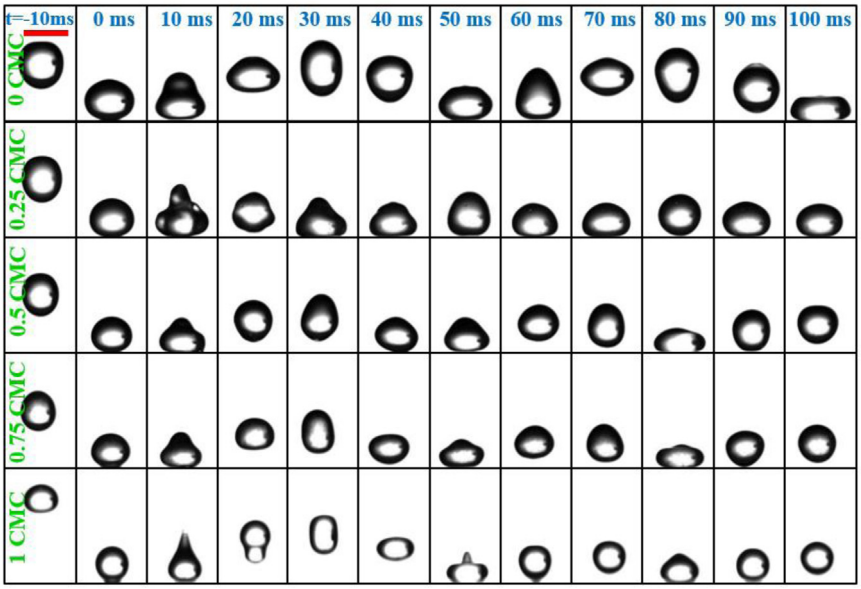

Fig. 9. Droplet trampolining dynamics of SDS solution droplets with low impact velocity $U = 0.5$ m/s at the surface temperature of 400 °C. The scale bar represents 2.64 mm. The dynamics of 1 CMC SDS droplets at 0.5 m/s, 0.75 m/s, and 1 m/s are presented in the supplementary section in movie format.

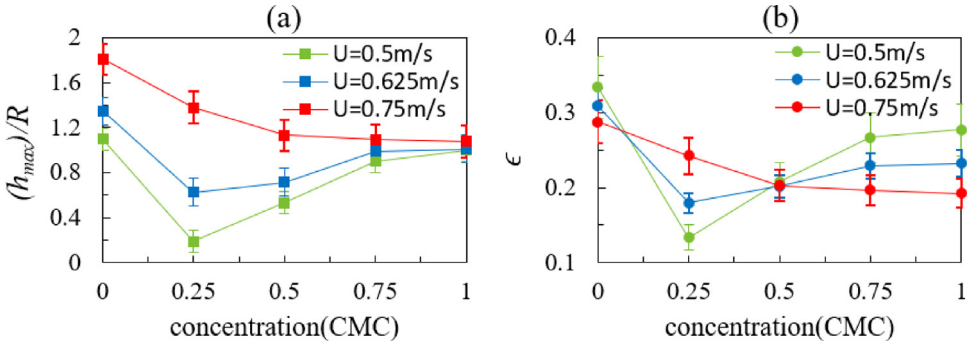

Fig. 10. **(a)** Non-dimensional rebound height vs. SDS concentrations for different impact velocities. Trampolining dynamics over time is presented as SI-5 (b) coefficient of restitution, ε, for the same process in (a).

creases with increase in concentration. This trend is similar to the trends of rebound heights presented in fig. SI-4 (0.5 m/sec). However, the rebound height measured for higher velocity (0.75 m/s) shows a monotonically decreasing trend with increasing surfactant concentration. Also, the non-dimensional rebound height is higher for 0.75 m/s velocity, unlike the trend presented in SI-4 at respective T_{DL} s. Compared to both 0.5 m/s and 0.625 cases, the frequency of rebound is reduced for 0.75 m/s (refer supplementary movies). The coefficient of restitution is defined as $\epsilon = \sqrt{\frac{h_{rebound}}{h_{impact}}}$. Fig. 10b presents the coefficient of restitution with variation in impact velocity and varying SDS concentrations. The ϵ is much less compared to the previous studies on Leidenfrost trampolining behavior where the ϵ was almost equal to 1 [42]. At a lower impact velocity, the coefficient decreases with concentration and then increases, and this behavior is observed in repeated experiments. At lower impact velocity, the low kinetic energy allows for better heat transfer and vapor generation due to greater contact time, which in turn promotes the Taylor instability at the droplet interface (refer Fig. 4b) [40]. Taylor instability promotes the formation of vapor dome and overall increase of vapor layer thickness. We speculate that the onset of this instability reduces the available kinetic energy during cushioning and rebound, leading to a reduced coefficient of restitution at lower concentrations. As the surfactant concentration increases, the effective spreading reduces. Consequently, the available interfacial area for the instability to manifest reduces, thereby reducing its strength. We postulate that, for this reason, the droplet is further able to exhibit an increased coefficient of restitution.

3.7. Fragmentation and jetting dynamics at ($T_s > T_{DL}$) ~400 °C

At higher impact velocity ~1 m/s and very high surface temperature, the droplets no longer stay intact and fragment into

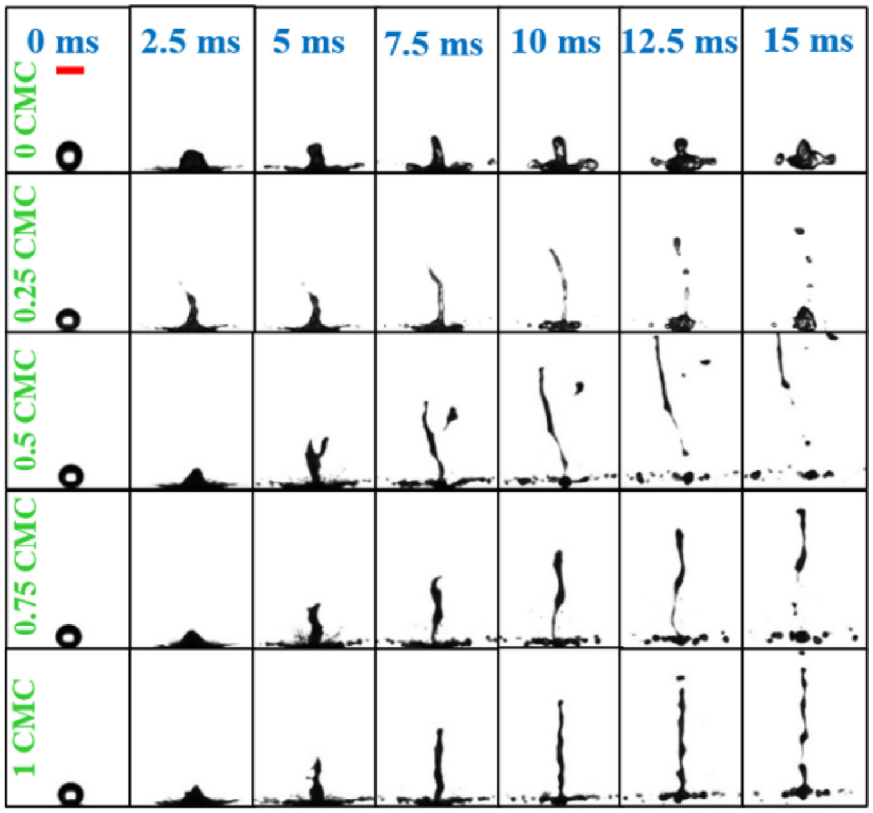

Fig. 11. Jet ejection dynamics of SDS solution droplets at high impact velocity $U = 1$ m/s for surface temperature ~400 °C. The scale bar represents 2.64 mm.

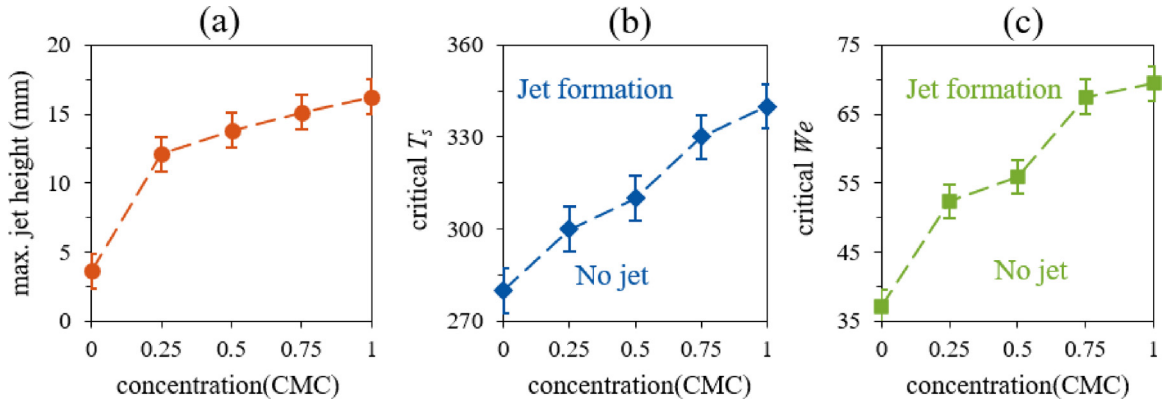

Fig. 12. Jet formation dynamics: (a) maximum jet height (b) critical substrate temperature (T_s) and (c) critical *We* with respect to SDS concentration of impinging droplets with high impact velocity $U = 1$ m/s at surface temperature 400 °C.

secondary droplets during the recoiling process after maximum spreading. This impact outcome is termed as explosive boiling. During retraction, the droplets undergo fragmentation into smaller droplets. The formation of a central jet was noticed and the height of the jet was observed to increase with the increase in SDS concentration (refer Fig. 11). It is noteworthy that due to higher impact velocity, the process of jet formation has started just after ~5 ms from the instant of the droplet touching the substrate, even before the attainment of maximum spread state. A previous study by Siddique et al. [43] showed that the jet formation was due to the inertial collapse of the air cavity formed beneath the droplet, caused by the rapid vaporization at the point of contact due to very high surface temperature. From Fig. 11 and Fig. 12a, it is evident that the central jet height increases with the increase of SDS concentration. For further description of jet ejection dynamics, the role of critical substrate temperature (T_S) and *We* at which the jet formation was observed for the first time has been highlighted in Fig. 12b and 12c, respectively. Fig. 12(b) reveals that the critical T_S increases with an increase of surfactant concentration. Fig. 12(c) shows that the critical *We* increases with an increase of surfactant (SDS) concentration. The higher surfactant concentration droplet has less surface tension than the low surfactant concentration droplet. When a droplet has low surface tension, it needs more stored kinetic energy to propagate the jet during the retraction phase. Similarly, the lesser stored kinetic energy is quite sufficient to support the onset of central-jet formation. Thus, higher surfactant (SDS) concentration droplets need higher critical T_S and large critical *We* to exhibit the onset of central jet-formation.

3.8. Boiling regimes of impacting surfactant droplets

Finally, we have presented the phase maps of different boiling regimes of the impacting water, SDS and CTAB solution droplets in Fig. 13a, b and c respectively. In case of SDS solution droplets (Fig. 13b), Leidenfrost temperature was attained at 240° C for 0.125 CMC and 290° C for 1 CMC concentration. For CTAB solution droplets the Leidenfrost temperature variation had a narrower range of 250° C (1 CMC) and 225° C (0.125 CMC). The parametric dependence of substrate temperature (150 °C - 400 °C) and Weber number based on the impact velocities (0.5 to 1 m/s) on the various boiling regimes is presented in Fig. 13. The surfactant concentrations ranged from 0.125CMC-1CMC for both CTAB and SDS solutions. The boiling regimes were distinguished into transition boiling, Leidenfrost state, trampolining behavior, and explosive boiling, marked with colored letters I (blue), II (red), III (pink), and IV (green), respectively in Fig. 13. In comparison to DI water droplets

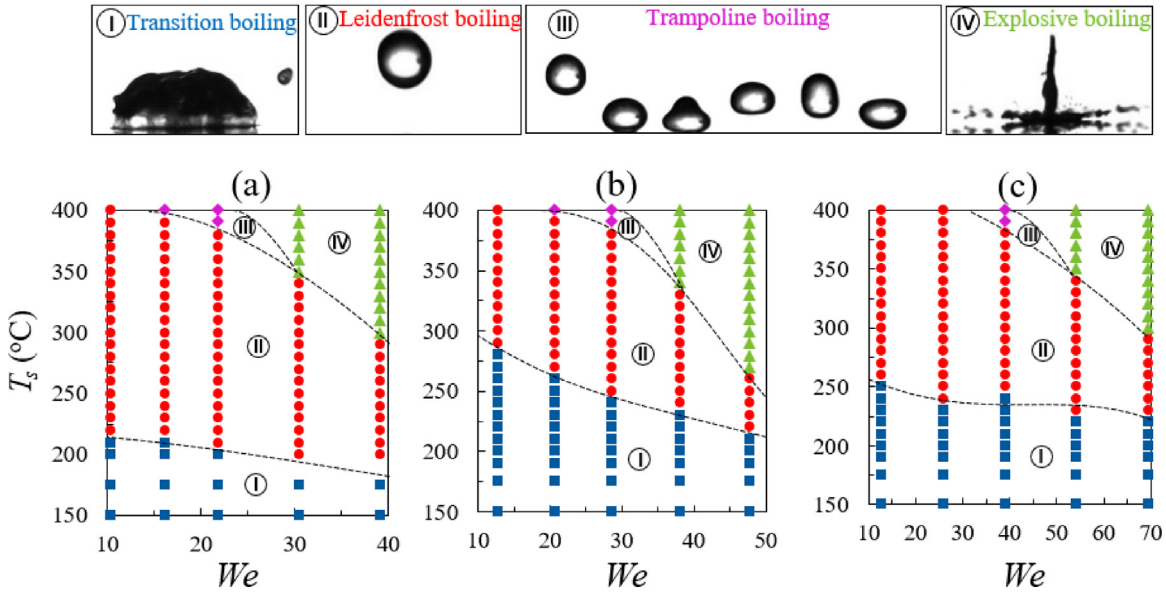

Fig. 13. Different boiling regimes impacting droplets of (a) water, (b) SDS, and (c) CTAB. The top row shows representative snapshots of the different boiling behaviors.

(see Fig. 13(a)), the phase diagram of SDS and CTAB droplets boiling behavior (presented in Fig. 13b & c respectively) highlights the greater coverage of transition boiling regime due to an increment of the T_{DL} with the addition of surfactants. In case of SDS solution droplets (Fig. 13b), the T_{DL} was attained at 240° C for 0.125 CMC and 290° C for 1 CMC concentration. For CTAB solution droplets the T_{DL} variation had a narrower range of 250° C (1 CMC) and 225° C (0.125 CMC). Also, the upper temperature limit of transition boiling reduces with *We* as T_{DL} was observed to decrease with *We*. Similarly, the explosive boiling region with central jet ejection is also occurring over a wider phase space due to higher chances of jet formation and fragmentation in the surfactant solutions. In this context, it is worthwhile to discuss the competition between both transition boiling and explosive boiling regimes against impact *We*. On the one hand, we notice that both SDS and CTAB solution droplets show the onset of transition boiling at lower substrate temperature even at higher *We*. On the other hand, explosive boiling exhibits at higher substrate temperatures even at low *We*. Thus, finally, from Fig. 13, the overall Leidenfrost regime is suppressed with an increase of surfactant concentration. For a specific fixed surfactant concentration, the Leidenfrost regime also shrinks (reduced shaded area) further with an increase in impact *We*.

4. Conclusions

The present study showed that both the surfactants (SDS and CTAB) are effective in increasing the Leidenfrost point T_{DL} compared to water. The T_{DL} was decreasing with Weber number for a fixed concentration, whereas, the T_{DL} was increasing with surfactant concentration. Scaling relationships of T_{DL} with *We* and *Oh* was proposed. At temperature significantly higher than T_{DL} (400° C), the drop impact behavior was shown to be dependent on the impact velocity. At lower impact velocity ~0.5 m/s, the droplets exhibited trampolining dynamics. On increasing the impact velocity ~1 m/s, droplets fragmented into secondary droplets along with the emergence of a vertical jet in the central region during the recoiling process. Finally, we have prepared a phase map of the different boiling states like transition, Leidenfrost, trampolining dynamics, and explosive boiling (with fragmentation and central jet formation) as a function of temperature and *We*. We believe our study will be helpful and instrumental in carrying out experiments and numerical simulations of surfactant droplet dynamics on heated substrates with further details. Also, the findings may have substantial implications in the design and development of safer and more reliable high-temperature thermal management strategies in certain niche utilities.

Data availability

All data pertaining to this research work are available in this article and the supporting information document.

Declaration of Competing Interest

The authors declare that they have no known competing financial interests or personal relationships that could have appeared to influence the work reported in this paper.

CRediT authorship contribution statement

Gudlavalleti VVS Vara Prasad: Investigation, Formal analysis, Writing – review & editing. **Purbarun Dhar:** Conceptualization, Project administration, Writing – review & editing. **Devranjan Samanta:** Conceptualization, Project administration, Writing – review & editing.

Acknowledgments

GVVSVP would like to thank the Ministry of Education, Govt. of India, for the doctoral scholarship. DS would like to thank IIT Ropar for partially funding the work (vide grant 9–246/2016/IITRPR/144). PD thanks IIT Kharagpur (vide grant SFI) and Science and Engineering Research Board (SERB) (vide grant SRG/2020/000004) for partially funding the work.

Supplementary materials

Supplementary material associated with this article can be found, in the online version, at doi:10.1016/j.ijheatmasstransfer.2022.122675.

References

[1] D. Quéré, Leidenfrost dynamics, Annu. Rev. Fluid Mech. 45 (2013) 197–215 September 2012, doi:10.1146/annurev-fluid-011212-140709.
[2] J.D. Bernardin, I. Mudawar, The leidenfrost point: Experimental study and assessment of existing models, J. Heat Transfer 121 (4) (1999) 894–903, doi:10.1115/1.2826080.
[3] G. Graeber, et al., Leidenfrost droplet trampolining, Nat. Commun. 12 (1) (2021) 1–7, doi:10.1038/s41467-021-21981-z.
[4] S.C. Yao, K.Y. Cai, The dynamics and leidenfrost temperature of drops impacting on a hot surface at small angles, Exp. Therm. Fluid Sci. 1 (4) (1988) 363–371, doi:10.1016/0894-1777(88)90016-7.
[5] I.U. Vakarelski, J.D. Berry, D.Y.C. Chan, S.T. Thoroddsen, Leidenfrost vapor layers reduce drag without the crisis in high viscosity Liquids, Phys. Rev. Lett. 117 (11) (2016) 1–5, doi:10.1103/PhysRevLett.117.114503.
[6] J. Cordeiro, S. Desai, The leidenfrost effect at the nanoscale, J. Micro Nano-Manufactur. 4 (4) (2016) 1–7, doi:10.1115/1.4034607.
[7] A.L. Biance, C. Clanet, D. Quéré, Leidenfrost drops, Phys. Fluids 15 (6) (2003) 1632–1637, doi:10.1063/1.1572161.
[8] H. Linke, et al., Self-propelled leidenfrost droplets, Phys. Rev. Lett. 96 (15) (2006) 2–5, doi:10.1103/PhysRevLett.96.154502.
[9] G. Lagubeau, M.Le Merrer, C. Clanet, D. Quéré, Leidenfrost on a ratchet, Nat. Phys. 7 (5) (2011) 395–398, doi:10.1038/nphys1925.
[10] G. Dupeux, M.Le Merrer, C. Clanet, D. Quéré, Trapping Leidenfrost drops with crenelations, Phys. Rev. Lett. 107 (11) (2011) 1–4, doi:10.1103/PhysRevLett.107.114503.
[11] A. Bouillant, T. Mouterde, P. Bourrianne, A. Lagarde, C. Clanet, D. Quéré, Leidenfrost wheels, Nat. Phys. 14 (12) (2018) 1188–1192, doi:10.1038/s41567-018-0275-9.
[12] M. Shirota, M.A.J. Van Limbeek, C. Sun, A. Prosperetti, D. Lohse, Dynamic Leidenfrost effect: relevant time and length scales, Phys. Rev. Lett. 116 (6) (2016) 1–5, doi:10.1103/PhysRevLett.116.064501.
[13] T. Tran, H.J.J. Staat, A. Prosperetti, C. Sun, D. Lohse, Drop impact on superheated surfaces, Phys. Rev. Lett. 108 (3) (2012) 1–5, doi:10.1103/PhysRevLett.108.036101.
[14] M. Khavari, C. Sun, D. Lohse, T. Tran, Fingering patterns during droplet impact on heated surfaces, Soft Matter 11 (17) (2015) 3298–3303, doi:10.1039/c4sm02878c.
[15] L. Rueda Villegas, S. Tanguy, G. Castanet, O. Caballina, F. Lemoine, Direct numerical simulation of the impact of a droplet onto a hot surface above the Leidenfrost temperature, Int. J. Heat Mass Transf. 104 (2017) 1090–1109, doi:10.1016/j.ijheatmasstransfer.2016.08.105.
[16] L. Qiao, Z. Zeng, H. Xie, H. Liu, L. Zhang, Modeling Leidenfrost drops over heated liquid substrates, Int. J. Heat Mass Transf. 128 (2019) 1296–1306, doi:10.1016/j.ijheatmasstransfer.2018.09.082.
[17] V. Bertola, K. Sefiane, Controlling secondary atomization during drop impact on hot surfaces by polymer additives, Phys. Fluids 17 (10) (2005), doi:10.1063/1.2112667.
[18] V. Bertola, An experimental study of bouncing Leidenfrost drops: comparison between newtonian and viscoelastic liquids, Int. J. Heat Mass Transf. 52 (7–8) (2009) 1786–1793, doi:10.1016/j.ijheatmasstransfer.2008.09.028.
[19] V. Bertola, Effect of polymer concentration on the dynamics of dilute polymer solution drops impacting on heated surfaces in the Leidenfrost regime, Exp. Therm. Fluid Sci. 52 (2014) 259–269, doi:10.1016/j.expthermflusci.2013.09.019.
[20] P. Dhar, S.R. Mishra, A. Gairola, D. Samanta, Delayed Leidenfrost phenomenon during impact of elastic fluid droplets: Leidenfrost phenomena, Proc. R. Soc. A Math. Phys. Eng. Sci. 476 (2243) (2020), doi:10.1098/rspa.2020.0556.
[21] P. Dhar, S.R. Mishra, D. Samanta, Onset of rebound suppression in non-Newtonian droplets post-impact on superhydrophobic surfaces, Phys. Rev. Fluids 4 (10) (2019) 103303, doi:10.1103/PhysRevFluids.4.103303.
[22] Y.M. Qiao, S. Chandra, Experiments on adding a surfactant to water drops boiling on a hot surface, Proc. R. Soc. A Math. Phys. Eng. Sci. 453 (1997) 673–689 1959, doi:10.1098/rspa.1997.0038.
[23] Y.M. Qiao, S. Chandra, Spray cooling enhancement by addition of a surfactant, J. Heat Transfer 120 (1) (1998) 92–98, doi:10.1115/1.2830070.
[24] H. Chen, W. long Cheng, Y. hang Peng, L. jia Jiang, Dynamic Leidenfrost temperature increase of impacting droplets containing high-alcohol surfactant, Int. J.

Heat Mass Transf. 118 (2018) 1160–1168, doi:10.1016/j.ijheatmasstransfer.2017.11.100.
[25] P. Zhang, B. Peng, X. Yang, J. Wang, L. Jiang, Regulating droplet dynamic wetting behaviors using surfactant additives on high-temperature surfaces, Adv. Mater. Interfaces 7 (14) (2020) 1–8, doi:10.1002/admi.202000501.
[26] F. Moreau, P. Colinet, S. Dorbolo, Explosive Leidenfrost droplets, Phys. Rev. Fluids 4 (1) (2019) 1–10, doi:10.1103/PhysRevFluids.4.013602.
[27] T. Kajiya, W. Kobayashi, T. Okuzono, M. Doi, Controlling the drying and film formation processes of polymer solution droplets with addition of small amount of surfactants, J. Phys. Chem. B 113 (47) (2009) 15460–15466, doi:10.1021/jp9077757.
[28] G. V V S Vara Prasad, P. Dhar, D. Samanta, Magneto-elastic effect in non-newtonian ferrofluid droplets impacting Superhydrophobic surfaces, Langmuir 37 (32) (2021) 9673–9682 Aug., doi:10.1021/acs.langmuir.1c00885.
[29] V. Bertola, An impact regime map for water drops impacting on heated surfaces, Int. J. Heat Mass Transf. 85 (2015) 430–437, doi:10.1016/j.ijheatmasstransfer.2015.01.084.
[30] J. Park, D.E. Kim, Dynamics of liquid drops levitating on superheated surfaces, Int. J. Therm. Sci. 152 (2020) 106321 November 2019, doi:10.1016/j.ijthermalsci.2020.106321.
[31] H. Hoffman, R. Sijs, T. De Goede, D. Bonn, Controlling droplet deposition with surfactants, Phys. Rev. Fluids 6 (3) (2021) 1–12, doi:10.1103/PhysRevFluids.6.033601.
[32] M. Aytouna, D. Bartolo, G. Wegdam, D. Bonn, S. Rafaï, Impact dynamics of surfactant laden drops: dynamic surface tension effects, Exp. Fluids 48 (1) (2010) 49–57, doi:10.1007/s00348-009-0703-9.
[33] X. Zhang, O.A. Basaran, Dynamic surface tension effects in impact of a drop with a solid surface, J. Colloid Interface Sci. 187 (1) (1997) 166–178, doi:10.1006/jcis.1996.4668.
[34] G. Chaniel, M. Frenkel, V. Multanen, E. Bormashenko, Paradoxical coffee-stain effect driven by the Marangoni flow observed on oil-infused surfaces, Colloid. Surf. A Physicochem. Eng. Asp. 522 (2017) 355–360, doi:10.1016/j.colsurfa.2017.03.009.
[35] R.T. van Gaalen, C. Diddens, H.M.A. Wijshoff, J.G.M. Kuerten, Marangoni circulation in evaporating droplets in the presence of soluble surfactants, J. Colloid Interface Sci. 584 (2021) 622–633, doi:10.1016/j.jcis.2020.10.057.
[36] D. Tam, V. von Arnim, G.H. McKinley, A.E. Hosoi, Marangoni convection in droplets on superhydrophobic surfaces, J. Fluid Mech. 624 (2009) 101–123, doi:10.1017/S0022112008005053.
[37] D. Liu, T. Tran, Size-dependent spontaneous oscillations of Leidenfrost droplets, J. Fluid Mech. (2020) December,, doi:10.1017/jfm.2020.576.
[38] A. Kaushal, V. Jaiswal, V. Mehandia, P. Dhar, Soluto-thermo-hydrodynamics influenced evaporation kinetics of saline sessile droplets, Eur. J. Mech. B/Fluids 83 (2020) 130–140, doi:10.1016/j.euromechflu.2020.04.014.
[39] A. Kaushal, V. Mehandia, P. Dhar, Ferrohydrodynamics governed evaporation phenomenology of sessile droplets, Phys. Fluids 33 (2) (2021), doi:10.1063/5.0040712.
[40] G. Paul, I. Manna, P.Kumar Das, Formation, growth, and eruption cycle of vapor domes beneath a liquid puddle during Leidenfrost phenomena, Appl. Phys. Lett. 103 (8) (2013), doi:10.1063/1.4819095.
[41] F. Celestini, T. Frisch, and Y. Pomeau, “Take Off of Small Leidenfrost Droplets,” vol. 034501, no. July, pp. 1–5, 2012, doi: 10.1103/PhysRevLett.109.034501.
[42] A. Jha, P. Chantelot, C. Clanet, D. Quéré, Viscous bouncing, Soft Matter 16 (31) (2020) 7270–7273, doi:10.1039/d0sm00955e.
[43] A.U. Siddique, M. Trimble, F. Zhao, M.M. Weislogel, H. Tan, Jet ejection following drop impact on micropillared hydrophilic substrates, Phys. Rev. Fluids 5 (6) (2020) 63606, doi:10.1103/PhysRevFluids.5.063606.